AAAS
Research
Volume 2019, Article ID 4152536, 10 pages
https://doi.org/10.34133/2019/4152536

Research Article

Virtually Wall-Less Tubular Sponges as Compartmentalized Reaction Containers

Shaohua Jiang[1], Viktoria Gruen[2], Sabine Rosenfeldt[2], Anna S. Schenk[2], Seema Agarwal[3], Zhi-Kang Xu[4], and Andreas Greiner[3,*]

[1] *College of Materials Science and Engineering, Nanjing Forestry University, Nanjing 210037, China*
[2] *Universität Bayreuth, Physical Chemistry, Universitätsstrasse 30, 95447 Bayreuth, Germany*
[3] *Universität Bayreuth, Macromolecular Chemistry, Bavarian Polymer Institute, Universitätsstrasse 30, 95440 Bayreuth, Germany*
[4] *MOE Key Laboratory of Macromolecular Synthesis and Functionalization, Key Laboratory of Adsorption and Separation Materials & Technologies of Zhejiang Province, Department of Polymer Science and Engineering, Zhejiang University, 310027 Hangzhou, China*

[*] Correspondence should be addressed to Andreas Greiner; greiner@uni-bayreuth.de

Received 18 November 2018; Accepted 10 March 2019; Published 30 May 2019

Sponges are open cellular materials with numerous interesting features. However, the potential of compartmentalized sponges has not been explored although many new properties and applications could be envisioned. We found that compartmentalized fibrous ultraporous polymer sponges with superhydrophobic surfaces could be designed as virtually wall-less reaction containers. With this, for example, the efficient removal of CO_2 from water and the controlled mineralization of calcium carbonate are possible. The high porosity (>99%) and superhydrophobicity make these sponges ideal candidates to hold alkanolamine solution for absorbing CO_2 and exchange gas through the walls of the sponges. The tubular sponge exhibits a much higher evaporation rate than a glass tube with the same diameter due to the much larger contact area between water and air. Therefore, the spongy reaction container also possesses a much faster adsorption rate, smaller equilibration time and higher efficiency for CO_2 adsorption than the glass tube container. In addition, these tubular sponges are also utilized to precipitate calcium carbonate by ammonium carbonate decomposition, which can control the deposition rates and products by tailoring the porosity and surface chemistry in the future. These new sponges provide an ideal basis for numerous new applications, for example, as breathable pipe lines for gas-liquid exchange, slag slurry carbonization, humidifier, and blood enricher.

1. Introduction

Open cellular fibrous materials are omnipresent in nature [1] and offer unique structure property relationships for man-made three-dimensional materials with numerous perspectives for applications. The most prominent examples of fibrous open cellular materials with interconnected pore structures are sponges [2]. Man-made sponges can be prepared following different concepts based on various materials [3, 4]. Ultralight sponges (density > 10 mg/cm^3, porosity > 99%) made of electrospun fibers are of particular interest. Recently, several groups reported on ultralight sponges based on the self-assembly of short electrospun polymer fibers from freeze-dried dispersions of the fibers [5–7] which provided numerous new property profiles. The conformal coating of ultralight sponges by chemical vapor deposition (CVD) of poly(p-xylylene) (PPX) resulted in superhydrophobic properties with improved mechanical integrity, solvent stability, and excellent insulation properties [8]. Further modification of ultralight sponges based on electrospun fibers could be extended to numerous new functions including drug release [9], tissue engineering [7, 10–14], oil-water separation [5, 6, 15], high temperature shielding [16, 17], electric conductivity [18], thermoresponsivity for water management [19], gelation agent [20], and catalysis for reactivity tuning [21].

In this contribution, we explored PPX-coated sponges with tubular shape. As a result, ultralight, low density, and open cellular tubes with highly porous walls with one or two open ends were obtained. These hollow sponges can hold aqueous solution without leakage although the walls are highly porous. The porosity is more than 99.5% which implies the walls are nothing but the network of open holes. The walls of these hollow sponges allow the free exchange of gas between the outside atmosphere and aqueous solution inside

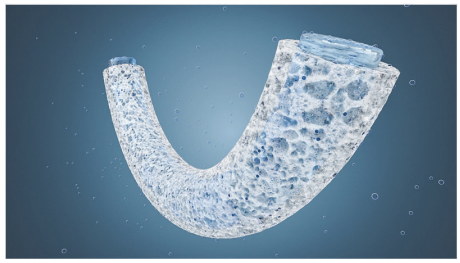

Figure 1: Schematic drawing of a tubular porous sponge. Gas bubbles penetrate the porous wall and can diffuse from the outer atmosphere towards the inner reaction channel.

the sponge as shown schematically in Figure 1. Containers or vessels with highly permeable walls for gases play an important role in nature, e.g., in lung and blood vessel and in technical systems, e.g., gas exchange membranes. In order to probe the versatility of these novel type of virtually wall-less hollow sponges for gas exchange we investigated qualitatively and quantitatively the sponges as a reaction containers for the efficient removal of gaseous CO_2 which is a major issue in technical plants [22–26] and for controlled mineralization of calcium carbonate where surface area may play a crucial role [27].

2. Results

2.1. Preparation and Morphology of Tubular Sponges. We designed tubular sponges as virtually wall-less reaction container following the process shown in Figure 2. The first step was the synthesis of a UV cross-linkable poly(methylacrylate-co-methyl methacrylate-co-4-methacryloyloxybenzophenone) (poly(MA-co-MMA-MABP)) followed by electrospinning of poly(MA-co-MMA-MABP) together with 14 wt% of polyacrylonitrile (PAN) and UV-crosslinking of the obtained fibers. The cross-linked fibers were cut to short fibers in dioxane which resulted a dispersion of short fibers (concentration of fibers = 4.7 mg/mL). The short fibers had an average fiber diameter of 1973 ± 185 nm and a length of 622 ± 279 μm (Figure 2(b)). Then the dispersion was transferred into a glass mold with one glass rod fixed in the center as a template for the tubular opening of the sponge. In order to get the container with one side sealed, a 3.5 cm length between the glass rod and the bottom of the glass tube was reserved. The dispersion in mold was frozen at -25°C, and then the glass rod was removed to form the hole in the center of the sponge. After drying at 0.34 mbar for 48 h, the as-prepared sponge (density: 5.69 mg/cm^3) with hollow column in the center and one end sealed was coated with a thin layer of PPX by CVD. After coating, the fiber diameter increased to 2664 ± 289 nm, implying an approx. 345 nm thickness of PPX coating around the fibers (Figure 2(c)). The PPX-coated hollow sponges (SG) showed an increased density of 9.26 mg/cm^3. The wall of the SG displayed hierarchical pore structure with big pores between the assembled aggregation of fibers (circles with yellow dashed line) and small pores in between the fibers (circle with red solid line) (Figure 2(c)). In spite of the low density and the highly porous character SG is mechanically very stable as demonstrated by manual squeezing (Movie S1).

2.2. Superhydrophobicity of SG. The superhydrophobic nature of the walls of the SG and their penetrability for water under atmospheric pressure was demonstrated by the placements of dyed water droplets on the inner side of the SG (Figures 3(a) and 3(b)). Even after complete filling of the center of the SG with dyed water no penetration of water through the walls was observed (Figure 3(c)). Cold water as well as hot water clearly does not penetrate the wall of the SG under atmospheric pressure as shown by thermal images (Figures 3(d) and 3(e)).

2.3. Gas-Liquid Exchange Capability of SG. The hierarchical porous structures of the SG wall provide exceptional path for gas exchange between the inside of the SG and the outer atmosphere which was proven experimentally by evaporation of liquid water from the inside of the SG with different inner diameter (7.0 and 14.0 mm). For comparison, standard glass tubes (GT) with 1 open end, which naturally have solid walls, with different inner diameters (4.5, 9.5, 12.5, 14.0, 15.5, and 19.5 mm) were used for the water evaporation experiment. As expected, the water evaporation was highly dependent on the diameter of the GT (Figure 4(a)). As the diameter of the GT increased from 4.5 to 19.5 mm, the water evaporation became faster and the corresponding evaporation rate increased from 0.0256 to 0.3357 mg/min. Due to the constant pressure (1 atm) and temperature (20°C), the difference of the evaporation rate could be attributed to the increased contact area of water to air. Figure 4(b) shows the relationship between the water evaporation rate and the contact area. The relationship could be described by a polynomial fitting with mono basic quadratic equation very well. In contrast, the SG exhibited significantly faster water evaporation than GT. The relationship between the amount of water evaporation and time was linear as well for SG (Figures 4(c) and 4(d)). The SG with inner diameter of 7 and 14 mm presented water evaporation rate of 0.5206 and 2.6846 mg/min, which were 3.5 and 18 times of that from GT with inner diameter of 14.0 mm and even 55% and 700% higher than that from GT with inner diameter of 19.5 mm. This by several orders of magnitude higher water evaporation rate from SG could be due to the larger contact area of water to air (Figure 4(e)). According to the polynomial fitting equation from Figure 4(b), the corresponding contact areas of water to air for the SG with inner diameter of 7 and 14 mm were 403.80 and 1105.48 mm^2, respectively, which are 162% and 618% higher than those of the GT with inner diameter of 14.0 mm.

In order to verify the excellent gas-liquid exchange capability of SG further in combination with a chemical reaction we performed a qualitative but very instructive experiment on CO_2 diffusion through the walls of the SG reaction container (Movie S2). As shown in Figure 5, 1.20 mL of saturated $Ca(OH)_2$/water solution with light red color dyed with phenolphthalein was filled in the SG and a standard

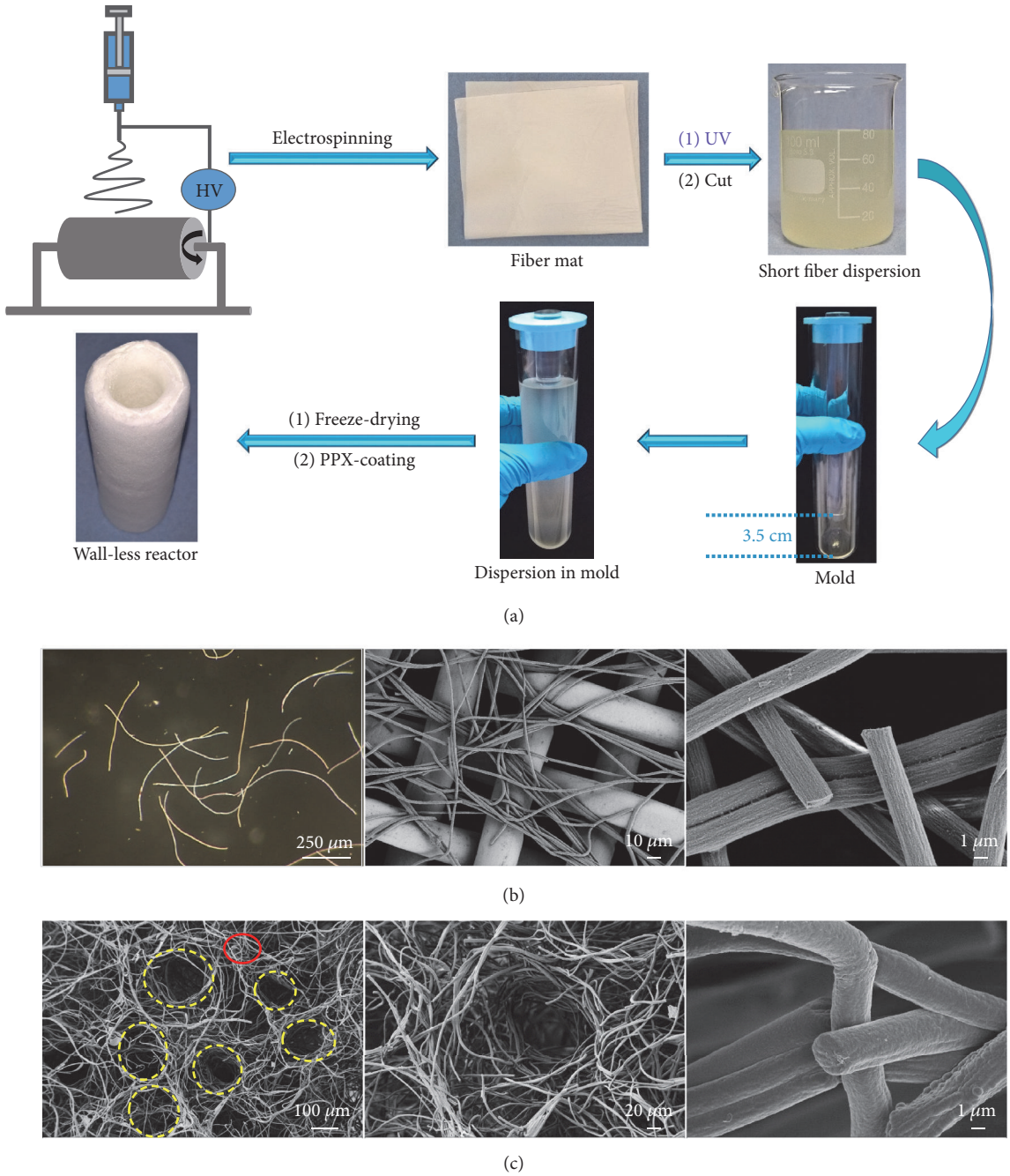

Figure 2: *Concept for the superhydrophobic porous reaction container.* (a) Illustrations of the preparation process leading to hollow sponges from electrospun fibers. (b) Morphology of the short electrospun fibers images by light microscopy and scanning electron microscopy. (c) Scanning electron micrographs showing the morphology of the hierarchical porous structures of the wall of the SG. Dashed circles with yellow and red color indicate the big and small pores, respectively.

glass vial for comparison. Both sides of the SG were sealed with a cover glass while the vial was open on the top. After the CO_2 was purged inside for approx. 2 min, the color of the solution in the SG became colorless indicating the alkaline solution became neutral or acidic solution due to the neutralization of $Ca(OH)_2$ with CO_2. In comparison, the solution in vial remained red indicating the solution was still alkaline. The difference on the reaction rate in the sponge reactor and in the vial could be attributed to the reaction contact area that the solution in the sponge possessed much higher contact area from the porous wall of the sponge while the solution in the vial only had the contact area on the top. This statement has to be proven quantitatively which was achieved by implementing the following set of experiments.

Verification of the above initial finding quantitatively with technically highly relevant removal of CO_2 by

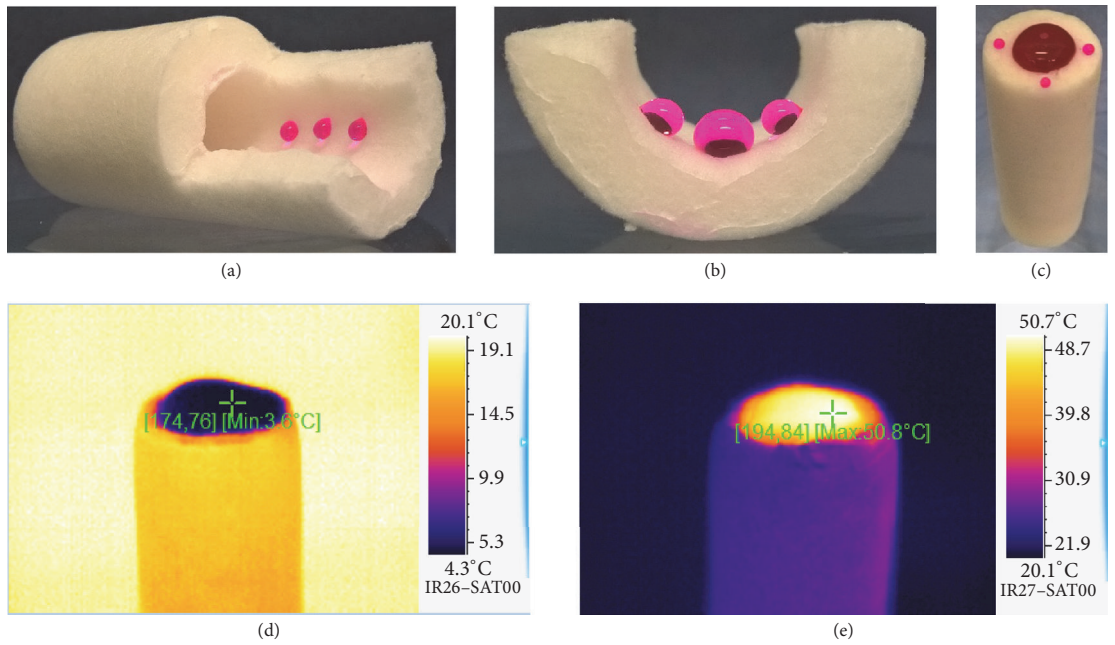

Figure 3: *Proof for superhydrophobic SG sponge walls.* (a) Photograph of small water droplets dyed by phenolphthalein inside the SG (opened by cutting). (b) Photograph of a cross-sectional view on the inside of a SG with big water droplets dyed by phenolphthalein. (c) Photograph of full water column (dyed with phenolphthalein) filling the center of the SG. (d) Thermal image of SG (one end closed) filled completely with cold water (dyed with phenolphthalein). (e) Thermal image of a SG (one end closed) filled completely with warm water (dyed with phenolphthalein).

Table 1: CO_2 adsorption rate (mol/kg/min) with SG and GT as containers at different time.

	SG-5	GT-5	SG-10	GT-10	SG-20	GT-20
5 min	0.02933	0.00745	0.03447	0.00827	0.05019	0.01028
15 min	0.01125	0.00449	0.01944	0.00578	0.02972	0.00909
30 min	0.00347	0.00342	0.00848	0.00478	0.01236	0.00649

diethanolamine (DEA) [28–31] in SG and GT both with inner diameter of 14.0 mm was performed at 5 bar and 20°C in an autoclave. The amount of CO_2 adsorption was determined by measuring the difference of the weight before and after the adsorption by an analytical balance with readability of 0.0001 g. Before the reaction, a blank experiment with water in SG and GT was carried out to evaluate the adsorption of CO_2 (Figure 6(a)). SG as container showed a fast initial CO_2 adsorption rate than the vial due to the quick gas transfer through the pores of SG. At the first 5 min, SG container exhibited CO_2 adsorption rate of 0.00756 mol/kg/min, which was nearly 4.0 times of that with GT as container (0.00192 mol/kg/min). Interestingly, during the observation time of 145 min, the CO_2 adsorption in SG container firstly increased. The highest CO_2 adsorption of 0.115 mol/kg was reached at 35 min, at which a saturation of CO_2 adsorption by water in SG was obtained. After that, the adsorption of CO_2 dropped down, which could be attributed to the fast release of CO_2 when the SG container was taken out for weight measurement.

Further experiment on CO_2 adsorption by DEA with concentrations of 5, 10, and 20 wt% in SG and GT was carried out at 5 bar and 20°C in an autoclave. The time dependent CO_2 adsorption and adsorption rate were illustrated in Figures 6(b) and 6(c) and Table 1. Due to the much higher adsorption of CO_2 by DEA than water, herein the CO_2 adsorption by the water in DEA solution was negligible. As expected, with the same DEA concentration, SG as reaction container exhibited much faster adsorption rate and equilibrium than GT. Taking 5 wt% DEA solution, for example, SG-5 only took 30 min while GT-5 needed more than 150 min to achieve the reaction equilibrium and the reaction rate in SG was 4 times of that in GT. These suggested the much higher efficiency of CO_2 adsorption by SG than GT. When we normalized the CO_2 adsorption efficiency by the amount of DEA, interestingly, the DEA solution with smaller concentration showed faster CO_2 adsorption rate and in general CO_2 adsorption rate with SG as container was faster than that with GT as container (Figure 6(d)).

2.4. Controlled Mineralization. To illustrate the use of our tubular sponges as highly versatile reaction containers in interface-mediated gas-diffusion reactions, we deposited calcium carbonate within the inner column of SG *via* the widely used ammonium carbonate diffusion technique [27]. For that purpose, SG filled with a reactant solution containing $CaCl_2$

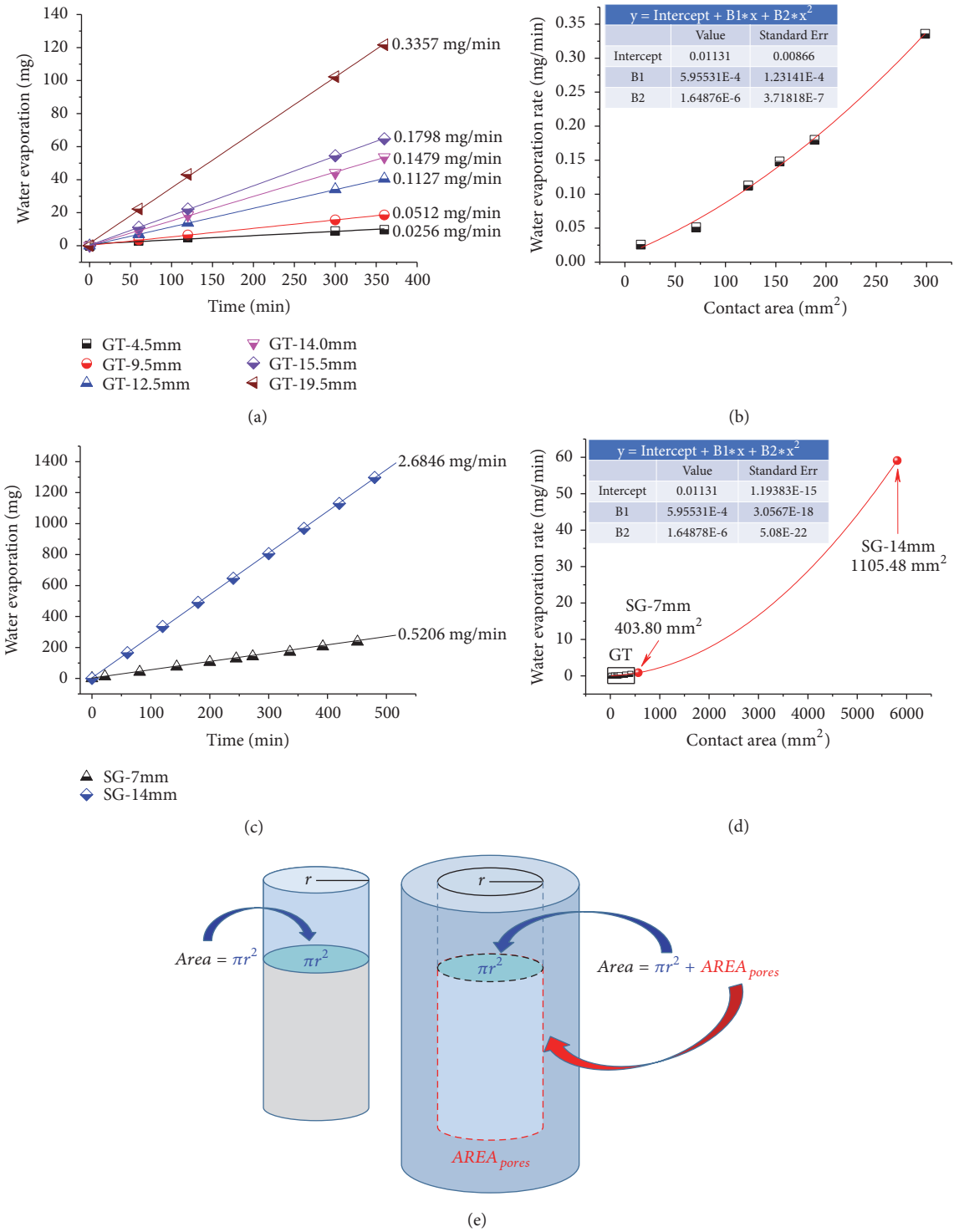

FIGURE 4: *Liquid water evaporation at 20°C from inside GT and SG.* (a) Time dependent water evaporation from glass tubes (GT) with different inner diameters. (b) Polynomial fitting on the water evaporation rate in GT and the contact area of water to air. (c) Time dependent water evaporation from SG. (d) Corresponding contact area of water to air in SG according to the polynomial fitting. (e) Illustration of the contact area of water to air in glass tube and hollow sponge.

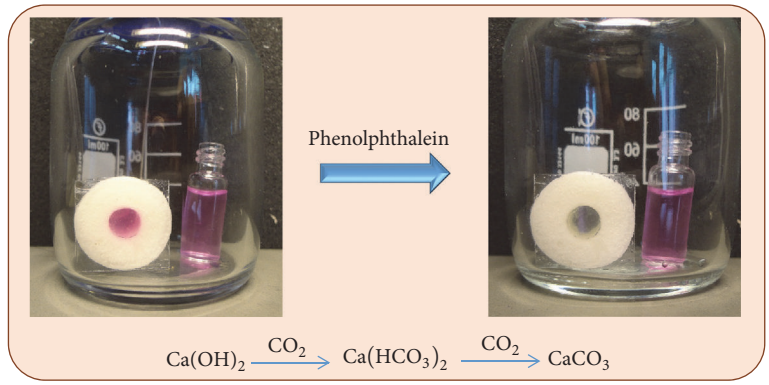

FIGURE 5: *Proof of gas-liquid exchange.* Neutralization reaction between CO_2 and $Ca(OH)_2$ monitored with phenolphthalein as a pH-sensitive indicator within a wall-less reaction container as compared to a glass vial.

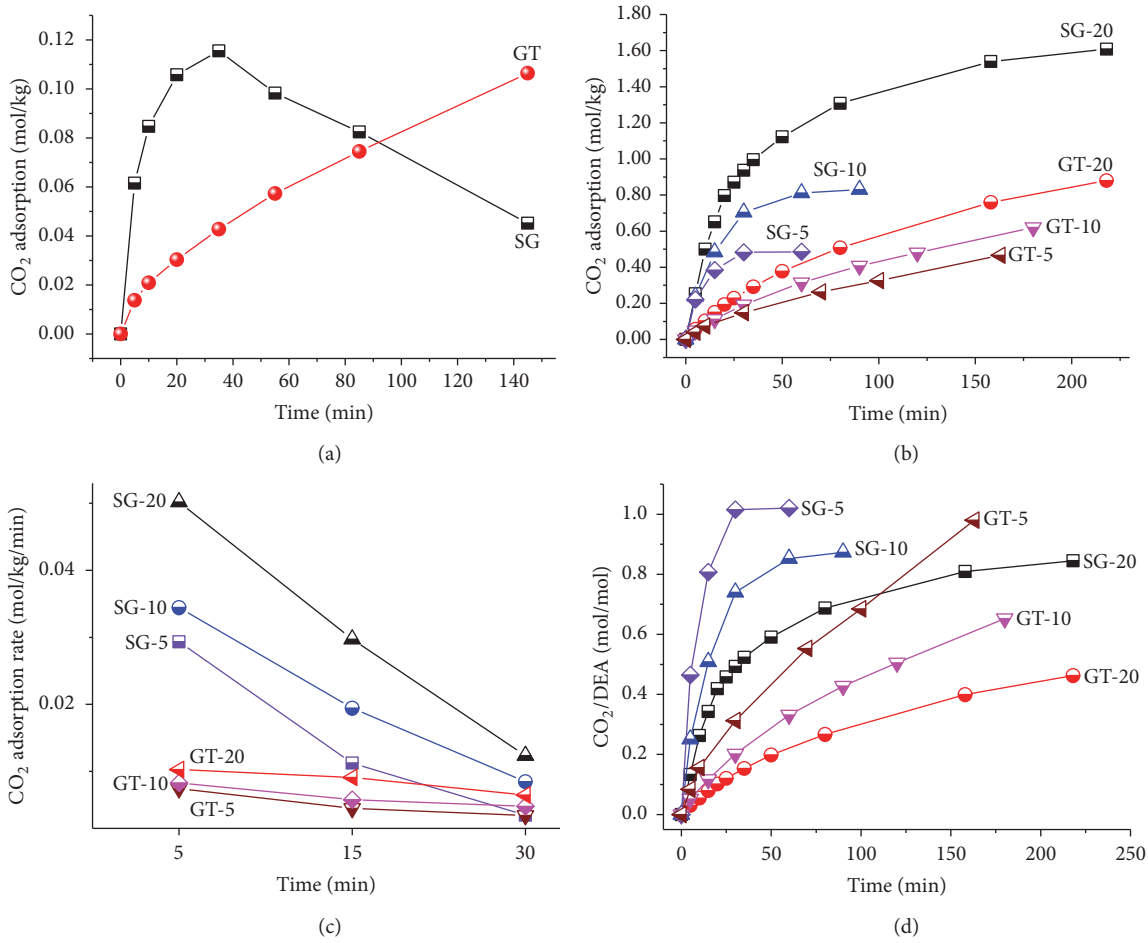

FIGURE 6: *CO_2 adsorption with SG and GT as containers at pressure of 5 bar.* (a) CO_2 adsorption by water with SG and GT as container. (b) CO_2 adsorption by DEA solutions with different concentrations of 5, 10, and 20 wt% with SG and GT as container. (c) CO_2 adsorption rate at 5, 15, and 30 min. (d) CO_2 solubility in DEA solutions with SG and GT as container.

and poly(acrylic acid) was exposed to a vapor phase composed of NH_3 and CO_2 formed by gradual decomposition of $(NH_4)_2CO_3$ at room temperature in a closed reaction chamber (Figure 7(a)). After completion of the reaction, the inner surface of the SG (Figure 7(b), red delineation) as well as its fibrous wall of (Figure 7(b), green dot) was examined. The solid precipitation appeared to be completely inhibited within the porous network of the container wall (Figure 7(c)). Energy-dispersive X-ray analysis (EDX) confirmed the absence of calcium, while $CaCO_3$ crystals were

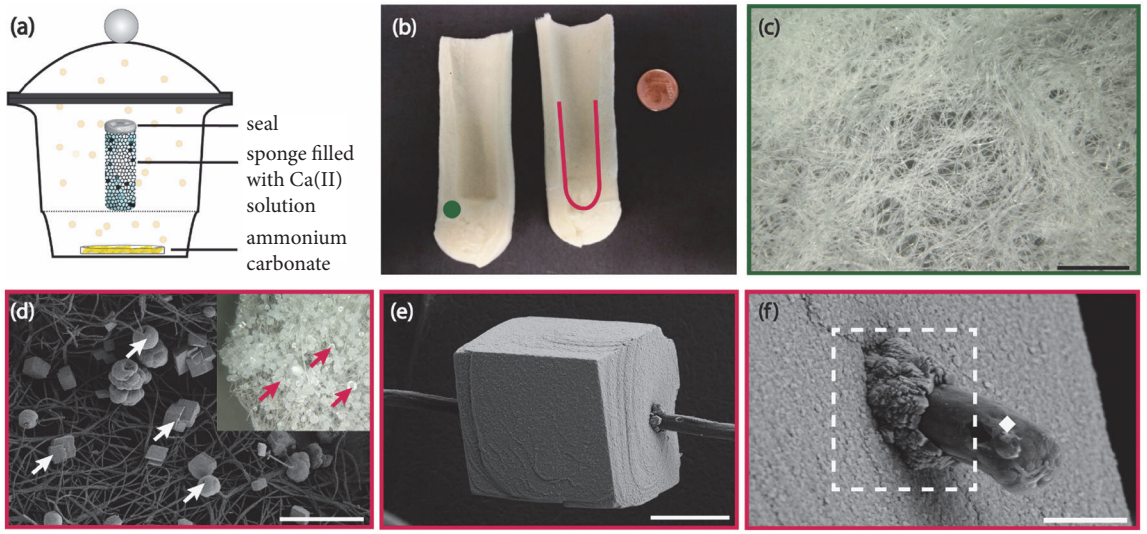

FIGURE 7: *Calcium carbonate precipitation within the tubular sponge reactor.* (a) Schematic illustration of the gas-diffusion setup used for $CaCO_3$ precipitation within hollow polymer tubes. (b) Photograph showing the longitudinal cross section of a sponge reactor after mineral deposition. The green dot marks the sponge wall, while the red line indicates the inner wall surface exposed to the reactant solution. (c) Light microscopy image of the polymer fibers within the tube wall (green dot in (b), scale bar = 200 μm). (d) Scanning electron micrograph showing calcium carbonate particles (indicated by white arrows) grown on the inner wall of the reaction channel (red delineation in (b), scale bar = 100 μm). Inset: overview image obtained by light microscopy demonstrating the full coverage of the channel surface with mineral particles (red arrows). (e) Rhombohedral calcium carbonate crystal grown around a polymer fiber (scale bar = 10 μm). (f) Scanning electron micrograph showing the position, where a polymer fiber (white diamond) protrudes from a calcium carbonate crystal. Small nanoscale particles mediate the contact between polymer and mineral within the interfacial region (dashed box, scale bar = 2 μm).

observed in large quantities in association with the polymer fibers at the inner surface of the reactor (Figures 7(d)–7(f)). The mineral particles deposited within the channel were mainly spherical or rhombohedral in shape (Figure 7(d)) and comprised a mixture of calcite and vaterite (C:V ≈ 88:12, Figure S1). These ~20 μm-sized crystals appeared to be threaded onto the sponge fibers (Figure 7(e)), where the interfacial contact was mediated by very small mineral particles (~200 nm) tightly associated with the polymer surface (Figure 7(f)).

Poly(acrylic acid) as a structure-directing additive has previously been shown to promote mineral precipitation according to a polymer-induced liquid precursor (PILP) mechanism [32, 33], where the polyelectrolyte stabilizes a highly hydrated amorphous precursor phase of calcium carbonate, which can wet surfaces [33] and infiltrate sub-micrometer pores by capillary action [34] before eventually crystallizing upon dehydration [35].

In our experiment carried out in virtually wall-less sponge reactors, however, the liquid-like mineral precursor, which is expected to form as an intermediate under the chosen conditions, was effectively prohibited from penetrating deep into the porous network due to the superhydrophobicity of the polymer fibers. Hence, in support of our hypothesis, mineral formation was restricted to the inner reaction channel of the hollow sponge container and the fibers themselves were nonwettable by the liquid-like amorphous mineral precursor. EDX mapping revealed that calcium ions were accumulated exclusively within the larger crystals and there was no signal attributed to the Ca Kα-line detected in the adjacent areas of the fiber (Figure S2). Therefore, nucleation of crystalline calcium carbonate occurred only locally in distinct spots on the fiber surface, which presumably coincide with small-scale defects in the PPX coating.

3. Discussion

In this work, we demonstrated a novel fibrous virtually wall-less hollow sponge based on electrospun fibers with high porosity and superhydrophobicity. The sponge can hold alkanolamine solution and exchange gas through the walls of the sponges. Compared to glass tubes with the same inner diameter of 14 mm, the hollow sponges have much faster water evaporation rates, which were 18 times of that from the glass tubes. The sponge as reaction container presents much faster adsorption rate to CO_2, which are up to 5 times of the reaction container of glass tubes when using the concentration of the diethanolamine in the range of 5-20 wt%. It could be envisioned that highly porous superhydrophobic sponges with numerous tubular channels could be utilized for highly efficient technical air purification of CO_2 or other acidic gases by diethanolamine or related reagents. The excellent gas permeability of the virtually wall-less sponge has additionally been utilized in the precipitation of calcium carbonate *via* ammonium carbonate decomposition. As the kinetics of this reaction are strongly governed by the transport of the gaseous reactants across the air/solution interface and thus by the diffusion profile and local supersaturation, the new hollow sponge provides the unique possibility of controlling deposition rates and products by tailoring the porosity and

surface chemistry of the fibrous polymer network. Intriguingly, even gradients with respect to gas permeability could be introduced into this highly flexible system by adjusting the processing parameters of the container. These sponges could also find applications in many other technological fields, for example, as humidifier and enrichers for blood.

4. Materials and Methods

4.1. Materials. Polyacrylonitrile (M_w = 150 000, Polyscience Inc.), [2.2] paracyclophane (parylene N, Speciality Coating Systems), dimethyl sulfoxide (DMSO, Fisher Chemical, 99.99%), dimethylformamide (DMF, Fisher Chemical, 99.99%), dioxane (technical grade), and acetone (technical grade), diethanolamine (DEA, 99.0%, Aldrich) were used as received. The monomers, methyl acrylate (MA, Aldrich, 99%) and methyl methacrylate (MMA, Aldrich, 99%) were purified by neutral aluminum oxide column before use. The initiator, 2,2'-azobis (isobutyronitrile) (AIBN, Fluka, 98%), was recrystallized from methanol (Aldrich, 99.8%). The cross-linker, 4-methacryloyloxybenzophenone (MABP), and the polymer, poly(MA-co-MMA-MABP) ($M_n = 2.43 \times 10^5$), were prepared according to our previous report [7].

4.2. Preparation of SG. The solution (22 wt%) for electrospinning was prepared by blending 25.28 g of poly(MA-co-MMA-co-MABP), 3.50 g of PAN, 46.50 g of DMSO, 35.50 g of DMF, and 20.50 g of acetone. The electrospinning parameters were high voltage (HV) of 20 kV, flow rate of 1.8 mL/h, collecting distance of 30 cm, and humidity of 40-60%. A rotating drum with diameter of 20 cm and rotation speed of 20 rpm was used to collect the electrospun fiber mats.

The obtained mats were first dried at room temperature for 14 h and then cross-linked by UV light (UV lamp 250GS) with an irradiation distance of 15 cm for 5 h for each side. Afterwards, the short fiber dispersion with concentration of 4.60 mg/mL was prepared by cutting the cross-linked fiber mat in dioxane with a razor blade at a rotation of 5000 rpm for 45 s. 80 mL of the dispersion was filled in the glass mold with inner diameter of 3.0 cm and one glass rod with a diameter of 1.4 cm placed in the middle. The dispersion in the mold was frozen at -25°C and dried by a freeze-drying machine (Christ Beta 2-16) at 0.34 mbar for 48 h to form the as-prepared sponge with hollow column in the middle.

4 pieces of the above sponges were put in the chemical vapor deposition chamber of coating machine. 2.0 g of [2.2] paracyclophane was sublimated at 150°C and become radical monomer gas by pyrolysis at 650°C. The monomer gas was cooled at 20°C under 35 mtorr and formed PPX coating on the fibers surface of the sponges with an average thickness of 390 nm.

4.3. Water Evaporation from SG. Different amount of water (1.00, 2.00, 5.00, 10.00, 10.00, and 20.00 g) was stored in GT with inner diameter of 4.5, 9.5, 12.5, 14.0, 15.5, and 19.5 mm while 1.50 and 10.00 g of water were stored in SG with inner diameter of 7.0 and 14.0 mm, respectively. All the above samples were put in a room with constant temperature of 20°C at approx. 1 atm. The weight changes from the water evaporation at different time were determined by an analytical balance with readability of 0.01 mg.

4.4. Chemical Reactions in SG. The initial attempt for the CO_2 involved reaction was performed with $Ca(OH)_2$. 1.20 mL of saturated light red $Ca(OH)_2$/water/phenolphthalein was filled in one SG container and vial. The SG (inner diameter of 7.0 mm; height of 1.5 cm) were sealed both sides with cover slide while the vial was not sealed by the cap. The SG and vial with $Ca(OH)_2$ solution were put in bottle with two needles to provide inlet and outlet of CO_2.

5, 10, and 20 wt% DEA/water solutions were prepared for the quantitate adsorption for CO_2 in SG and GT. The SG and GT had the same inner diameter of 14.0 mm. The SG and GT containing 10.0 g of the DEA solutions were sealed in an autoclave in which 5 bar of CO_2 was applied. After different time, the increased weight of the solutions by the adsorption of CO_2 was measured by an analytical balance with readability of 0.0001 g at different time interval. With the increased weight from the adsorption of CO_2, the corresponding molar values of CO_2 could be obtained.

Calcium carbonate was deposited within a wall-less reaction container by filling the hollow sponge with 10 mL of a 20 mM solution of $CaCl_2 \cdot 2H_2O$ (Sigma-Aldrich). Poly(acrylic acid) (10 μg/mL, M_W ~100 000 g/mol, 35 wt% in H_2O, Sigma-Aldrich) was added as a structure-directing additive to promote crystallization *via* a polymer-induced liquid precursor [32, 33]. Precipitation of the mineral phase was induced by exposing the reactant solution to ammonium carbonate vapor within a closed desiccator (Figure 7(a)). The open end of the tubular sponge was sealed such that diffusion of the gaseous reagents into the Ca(II)-solution was restricted to the porous polymer network. After 2 days of reaction time the sponge was removed from the reaction chamber and the inner channel was washed with deionized water and ethanol and subsequently left to dry under ambient conditions. The mineral precipitates formed at the inner wall of the hollow sponge were characterized by optical microscopy (VHX-950F, Keyence) and scanning electron microscopy (LEO 1530 Gemini, Zeiss) in combination with energy-dispersive X-ray spectroscopy (Thermo Fisher Scientific NS7). Powder X-ray diffractograms were recorded in Bragg Brentano geometry as coupled θ-2θ scans spanning an angular range of $20^\circ < 2\theta < 85^\circ$. Measurements were performed with an Empyrean system (PANalytical, Almelo, Netherlands) equipped with a sealed X-ray tube (Cu-Kα, Ni-filtered) and a PIXEL solid state detector.

Conflicts of Interest

The authors declare that there are no conflicts of interest regarding the publication of this article.

Authors' Contributions

Shaohua Jiang, Viktoria Gruen, Sabine Rosenfeldt, and Anna S. Schenk designed and performed the experiments. Seema Agarwal and Zhi-Kang Xu gave many suggestions. Andreas

Greiner was in charge for the whole project. All the authors wrote the manuscript and contributed to discussions.

Acknowledgments

We thank the Bavarian Polymer Institute (BPI) for providing access to electron microscopy facilities. Donation of Dimer N by Speciality Coating Systems is kindly acknowledged. This work was supported by the University of Bayreuth, the DFG via Collaborative Research Center SFB 840, the DFG GIP Project, the National Natural Science Foundation of China (51803093), and the Natural Science Foundation of Jiangsu Province of China (BK20180770).

Supplementary Materials

Movie S1: mechanically stable sponge to resist manual squeezing. *Movie S2*: comparative experiment for the adsorption of CO_2 using sponge and glass tube as reaction container. *Figure S1: Powder X-ray diffraction analysis of SG.* (a) Diffractograms of the polymer sponges were obtained before (red squares, SG pure) and after (blue circles, SG loaded) mineral deposition. The reaction container in its original state showed only 2 broad halos as they are characteristic of polymeric compounds. In contrast, the sponge piece which had been cut out from the mineralized channel surface after exposure to ammonium carbonate vapor exhibited distinct Bragg peaks indicating the presence of crystalline particles. The PXRD pattern of the deposited calcium carbonate mineral (black line, background corrected) was obtained after subtraction of a normalized SG pure background profile from the curve of the loaded container. (b) After background subtraction the diffraction profile of the mineralized sponge (inner channel surface, black triangles) could be assigned to a mixture of calcite (thick red line) and vaterite (thin blue line) using the software X'Pert High Score Plus 3.0 (PANalytical). The intensities of the (104)-peak of calcite and the (101)-peak of vaterite were used to roughly estimate the ratio of calcite to vaterite. For that purpose, the (104) Bragg peak of calcite was normalized to I(2θ) = 100 counts and the resulting pattern was compared with reference data obtained from rhombohedral calcite (ICDD-PDF reference code 01-085-0849) and hexagonal vaterite (ICDD-PDF reference code 00-024-0030) yielding a ratio of ca. 88% calcite and 12 % vaterite. *Figure S2: EDX analysis of a representative area on the inner surface of the sponge reaction container.* (a) Scanning electron micrograph of a calcium carbonate crystal (red asterisk) deposited around polymer fibers within the inner lining of the container wall (white arrows). The contact area between the micron-scale particle and the organic fiber is lined with smaller crystallites (blue circle). (b) Corresponding EDX-map showing the distribution of calcium in the same area. The intensity of the signal attributable to the Ca Kα-line was mapped in steps of 0.19 μm at an acceleration voltage of 10 kV. *(Supplementary Materials)*

References

[1] L. J. Gibson and M. F. Ashby, *Cellular Solids: Structure and Properties*, Cambridge University Press, Cambridge, UK, 1999.

[2] S. P. Leys and A. Hill, "The Physiology and Molecular Biology of Sponge Tissues," *Advances in Marine Biology*, vol. 62, pp. 1–56, 2012.

[3] S. Jiang, S. Agarwal, and A. Greiner, "Low-density open cellular sponges as functional materials," *Angewandte Chemie International Edition*, vol. 56, no. 49, pp. 15520–15538, 2017.

[4] S. Zhao, W. J. Malfait, N. Guerrero-Alburquerque, M. M. Koebel, and G. Nyström, "Biopolymer aerogels and foams: chemistry, properties, and applications," *Angewandte Chemie International Edition*, vol. 57, no. 26, pp. 7580–7608, 2018.

[5] Y. Si, J. Yu, X. Tang, J. Ge, and B. Ding, "Ultralight nanofibre-assembled cellular aerogels with superelasticity and multifunctionality," *Nature Communications*, vol. 5, 2014.

[6] F. Deuber, S. Mousavi, M. Hofer, and C. Adlhart, "Tailoring pore structure of ultralight electrospun sponges by solid templating," *ChemistrySelect*, vol. 1, no. 18, pp. 5595–5598, 2016.

[7] G. Duan, S. Jiang, V. Jérôme et al., "Ultralight, soft polymer sponges by self-assembly of short electrospun fibers in colloidal dispersions," *Advanced Functional Materials*, vol. 25, no. 19, pp. 2850–2856, 2015.

[8] G. Duan, S. Jiang, T. Moss, S. Agarwal, and A. Greiner, "Ultralight open cell polymer sponges with advanced properties by PPX CVD coating," *Polymer Chemistry*, vol. 7, no. 15, pp. 2759–2764, 2016.

[9] G. Duan, A. R. Bagheri, S. Jiang, J. Golenser, S. Agarwal, and A. Greiner, "Exploration of macroporous polymeric sponges as drug carriers," *Biomacromolecules*, vol. 18, no. 10, pp. 3215–3221, 2017.

[10] T. Xu, J. M. Miszuk, Y. Zhao, H. Sun, and H. Fong, "Electrospun polycaprolactone 3D nanofibrous scaffold with interconnected and hierarchically structured pores for bone tissue engineering," *Advanced Healthcare Materials*, vol. 4, no. 15, pp. 2238–2246, 2015.

[11] Q. Yao, J. G. L. Cosme, T. Xu et al., "Three dimensional electrospun PCL/PLA blend nanofibrous scaffolds with significantly improved stem cells osteogenic differentiation and cranial bone formation," *Biomaterials*, vol. 115, pp. 115–127, 2017.

[12] B. Sun, Z. Zhou, T. Wu et al., "Development of nanofiber sponges-containing nerve guidance conduit for peripheral nerve regeneration in vivo," *ACS Applied Materials & Interfaces*, vol. 9, no. 32, pp. 26684–26696, 2017.

[13] J. M. Miszuk, T. Xu, Q. Yao et al., "Functionalization of PCL-3D electrospun nanofibrous scaffolds for improved BMP2-induced bone formation," *Applied Materials Today*, vol. 10, pp. 194–202, 2018.

[14] M. Mader, V. Jérôme, R. Freitag, S. Agarwal, and A. Greiner, "Ultraporous, compressible, wettable polylactide/polycaprolactone sponges for tissue engineering," *Biomacromolecules*, vol. 19, no. 5, pp. 1663–1673, 2018.

[15] Y. Liu, Y. Peng, T. Zhang, F. Qiu, and D. Yuan, "Superhydrophobic, ultralight and flexible biomass carbon aerogels derived from sisal fibers for highly efficient oil–water separation," *Cellulose*, vol. 25, no. 5, pp. 3067–3078, 2018.

[16] S. Jiang, B. Uch, S. Agarwal, and A. Greiner, "Ultralight, thermally insulating, compressible polyimide fiber assembled sponges," *ACS Applied Materials & Interfaces*, vol. 9, no. 37, pp. 32308–32315, 2017.

[17] H. Wang, X. Zhang, N. Wang et al., "Ultralight, scalable, and high-temperature–resilient ceramic nanofiber sponges," *Science Advances*, vol. 3, no. 6, p. e1603170, 2017.

[18] S. Jiang, S. Reich, B. Uch, P. Hu, S. Agarwal, and A. Greiner, "Exploration of the electrical conductivity of double-network silver nanowires/polyimide porous low-density compressible sponges," *ACS Applied Materials & Interfaces*, vol. 9, no. 39, pp. 34286–34293, 2017.

[19] S. Jiang, N. Helfricht, G. Papastavrou, A. Greiner, and S. Agarwal, "Low-Density self-assembled poly(N-isopropyl acrylamide) sponges with ultrahigh and extremely fast water uptake and release," *Macromolecular Rapid Communications*, vol. 39, no. 8, 2018.

[20] S. Jiang, G. Duan, U. Kuhn et al., "Spongy gels by a top-down approach from polymer fibrous sponges," *Angewandte Chemie International Edition*, vol. 56, no. 12, pp. 3285–3288, 2017.

[21] G. Duan, M. Koehn-Serrano, and A. Greiner, "Highly efficient reusable sponge-type catalyst carriers based on short electrospun fibers," *Macromolecular Rapid Communications*, vol. 38, no. 3, Article ID 1600511, 2017.

[22] A. Timmermann, J. Oberhuber, A. Bacher, M. Esch, M. Latif, and E. Roeckner, "Increased El Nino frequency in a climate model forced by future greenhouse warming," *Nature*, vol. 398, no. 6729, pp. 694–697, 1999.

[23] F. M. Nick, A. Vieli, M. L. Andersen et al., "Future sea-level rise from Greenland's main outlet glaciers in a warming climate," *Nature*, vol. 497, no. 7448, pp. 235–238, 2013.

[24] J. M. Gregory and J. Oerlemans, "Simulated future sea-level rise due to glacier melt based on regionally and seasonally resolved temperature changes," *Nature*, vol. 391, no. 6666, pp. 474–476, 1998.

[25] T. C. Paulitz and R. R. Bélanger, "Biological control in greenhouse systems," *Annual Review of Phytopathology*, vol. 39, pp. 103–133, 2001.

[26] S. H. Schneider, "The greenhouse effect: science and policy," *Science*, vol. 243, no. 4892, pp. 771–781, 1989.

[27] J. Ihli, P. Bots, A. Kulak, L. G. Benning, and F. C. Meldrum, "Elucidating mechanisms of diffusion-based calcium carbonate synthesis leads to controlled mesocrystal formation," *Advanced Functional Materials*, vol. 23, no. 15, pp. 1965–1973, 2013.

[28] B. Lv, B. Guo, Z. Zhou, and G. Jing, "Mechanisms of CO_2 capture into monoethanolamine solution with different CO_2 loading during the absorption/desorption processes," *Environmental Science & Technology*, vol. 49, no. 17, pp. 10728–10735, 2015.

[29] M. Rahbari-Sisakht, A. F. Ismail, D. Rana, and T. Matsuura, "Carbon dioxide stripping from diethanolamine solution through porous surface modified PVDF hollow fiber membrane contactor," *Journal of Membrane Science*, vol. 427, pp. 270–275, 2013.

[30] B. Dutcher, M. Fan, and A. G. Russell, "Amine-based CO2 capture technology development from the beginning of 2013-A review," *ACS Applied Materials & Interfaces*, vol. 7, no. 4, pp. 2137–2148, 2015.

[31] S. A. Mazari, B. Si Ali, B. M. Jan, I. M. Saeed, and S. Nizamuddin, "An overview of solvent management and emissions of amine-based CO2 capture technology," *International Journal of Greenhouse Gas Control*, vol. 34, pp. 129–140, 2015.

[32] L. B. Gower, "Biomimetic model systems for investigating the amorphous precursor pathway and its role in biomineralization," *Chemical Reviews*, vol. 108, no. 11, pp. 4551–4627, 2008.

[33] X. Xu, J. T. Han, and K. Cho, "Formation of amorphous calcium carbonate thin films and their role in biomineralization," *Chemistry of Materials*, vol. 16, no. 9, pp. 1740–1746, 2004.

[34] Y.-Y. Kim, N. B. J. Hetherington, E. H. Noel et al., "Capillarity creates single-crystal calcite nanowires from amorphous calcium carbonate," *Angewandte Chemie International Edition*, vol. 50, no. 52, pp. 12572–12577, 2011.

[35] S. E. Wolf and L. B. Gower, *Challenges And Perspectives of The Polymer-Induced Liquid-Precursor Process: The Pathway from Liquid-Condensed Mineral Precursors to Mesocrystalline Products. in New Perspectives on Mineral Nucleation And Growth: from Solution Precursors to Solid Materials*, A. E. S. Van Driessche, M. Kellermeier, L. G. Benning, and D. Gebauer, Eds., Springer International Publishing, Cham, Switzerland, 2017.